Contemporary continuum QCD approaches to excited hadrons

Bruno El-Bennich[1,2,a] and Eduardo Rojas[3,b]

[1]*Laboratório de Física Teórica e Computacional, Universidade Cruzeiro do Sul, Rua Galvão Bueno 868, 01506-000 São Paulo, SP, Brazil*
[2]*Instituto de Física Teórica, Universidade Estadual Paulista, Rua Bento Teobaldo Ferraz 271, 01140-070 São Paulo, SP, Brazil*
[3]*Instituto de Física, Universidad de Antioquia, Calle 70, no. 52-21, Medellín, Colombia*

Abstract. Amongst the bound states produced by the strong interaction, radially excited meson and nucleon states offer an important phenomenological window into the long-range behavior of the coupling constant in Quantum Chromodynamics. We here report on some technical details related to the computation of the bound state's eigenvalue spectrum in the framework of Bethe-Salpeter and Faddeev equations.

1 Introduction: excited states as an eigenvalue problem

A great deal of research activity in hadron physics is concerned with hadron structure and revolves around two fundamental questions: what constituents are the hadrons made of and how does Quantum Chromodynamics (QCD), the strong interaction component of the Standard Model, produce them? These are simple questions which, however, may not entail simple answers. To understand the measurable content of QCD, spectroscopy is a valuable and time-honored tool — suffice it to mention the inestimable progress made in the computation of atomic or molecular spectra and subsequent comparison with experiments that lead to a deeper understanding of Quantum Electrodynamics.

The same is true for QCD: if confinement is related to the analytic properties of QCD's Schwinger functions, then light-quark confinement ought to be understood by mapping out the infrared behavior of the theory's universal β function. Obviously, this cannot be possibly achieved in perturbation theory. A nonperturbative continuum approach to QCD is provided by Dyson-Schwinger equations (DSE) which relate the theory's β function to experimental observables [1]. Therefore, comparison between DSE predictions embedded in bound-state calculations and observations of the hadron mass spectrum as well as of elastic and transition form factors can be used to study the long-range behavior of QCD's interaction. As the properties of excited hadron states are considerably more sensitive to the long-range behavior of the strong interaction than those of ground states [2–4], excited mesons and nucleons [5] are an important source of information and complement our understanding of the strong interaction in light mesons [6–9] and in heavy-light mesons with disparate energy scales [10–13].

Of course, the properties of these hadrons can only be understood, and the functional behavior of the β function be inferred therefrom, by studying the quark's DSE in conjunction with quark-antiquark

[a]e-mail: bruno.bennich@cruzeirodosul.edu.br

[b]e-mail: eduardo.rojas@cruzeirodosul.edu.br

or three-quark bound-state equations, the Bethe-Salpeter and Faddeev equations, respectively. Both are treated as eigenvalue problems which we here exemplify with the relativistic bound-state equation of pseudoscalar $J^P = 0^-$ mesons. The homogeneous Bethe-Salpeter equation for this $q\bar{q}$ bound state with relative momentum p and total momentum P can be generally written as,

$$\Gamma_{0^-}(p, P) = \int_k^\Lambda \mathcal{K}(p, k, P) \left[S(k + \eta_+ P) \, \Gamma_{0^-}(k, P) \, S(k - \eta_- P) \right] , \tag{1}$$

where $S(k \pm \eta_\pm P)$ are dressed quark propagators with $\eta_+ + \eta_- = 1$ (NB: in a Poincaré invariant calculation numerical results are independent of the momentum partition parameter $\eta_\pm$). For the sake of simplicity, we omit flavor and Dirac indices, as the following discussion is independent of them. In the same spirit, we restrict ourselves to the rainbow-ladder truncation of the interaction kernel,

$$\mathcal{K}(p, k, P) = -\frac{Z_2^2 \, \mathcal{G}(q^2)}{q^2} \frac{\lambda^a}{2} \gamma_\mu T_{\mu\nu}(q) \frac{\lambda^a}{2} \gamma_\nu , \tag{2}$$

with the transverse projection operator $T_{\mu\nu}(q) := g_{\mu\nu} - q_\mu q_\nu / q^2$, $q = p - k$, Z_2 is the wave-function renormalization constant and λ^a are the SU(3) color matrices in the fundamental representation. Various model ansätze [14–17] have been proposed for the effective interaction, $\mathcal{G}(q^2)$, which emulates the combined effect of the gluon and quark-gluon vertex dressing functions and most recent efforts extend these models to include important transverse components of this vertex beyond the leading truncation [18]. Most importantly, Eq. (2) satisfies the axialvector Ward-Takahashi identity [19] and therefore ensures a massless pion in the chiral limit. As we shall see below, Eqs. (1) and (2) define an eigenvalue problem with physical solutions at the mass-shell points, $P^2 = -m^2$, where m is the bound-state mass.

The Bethe-Salpeter equation's Poincaré-invariant solutions can be cast in the form,

$$\Gamma_{0^-}(p, P) = \gamma_5 \left[i \mathbb{I}_D E_{0^-}(p, P) + \slashed{P} F_{0^-}(p, P) + \slashed{p}(p \cdot P) G_{0^-}(p, P) + \sigma_{\mu\nu} p_\mu P_\nu \, H_{0^-}(p, P) \right] , \tag{3}$$

Note that this Euclidean-metric basis, $\mathcal{A}^\alpha(p, P) = \gamma_5\{i \mathbb{I}_D, \slashed{P}, \slashed{p}(p \cdot P), \sigma_{\mu\nu} p_\mu P_\nu\}$, is nonorthogonal with respect to the Dirac trace. The functions $\mathcal{F}_{0^-}^\alpha(p, P) = \{E_{0^-}(p, P), F_{0^-}(p, P), G_{0^-}(p, P), H_{0^-}(p, P)\}$ are Lorentz-invariant scalar amplitudes and are extracted from the Bethe-Salpeter amplitude (3) with appropriate projectors, $P^a(p, P)$,[1]

$$\tfrac{1}{4} P^{\alpha\beta}(p, P) \, \mathrm{Tr}_D \left[\mathcal{A}^\beta(p, P) \mathcal{A}^\gamma(p, P) \right] = \delta_{\alpha\gamma} ; \quad P^\alpha(p, P) = P^{\alpha\beta}(p, P) \, \mathcal{A}^\beta(p, P) , \tag{4}$$

where $\alpha, \beta = 1, ..., 4$ and the projection is given by:

$$\mathcal{F}_{0^-}^\alpha(p, P) = \tfrac{1}{4} \mathrm{Tr}_D \left[P^\alpha(p, P) \, \Gamma_{0^-}(p, P) \right] . \tag{5}$$

Using the Bethe-Salpeter equation, this leads to the eigenvalue problem,

$$\lambda(P^2) \mathcal{F}_{0^-}^\alpha(p, P) = \int_k^\Lambda \mathcal{K}^{\alpha\beta}(p, k, P) \mathcal{F}_{0^-}^\beta(k, P) , \tag{6}$$

where $\mathcal{K}^{\alpha\beta}(p, k, P)$ stems from the projection of Eq. (1) using Eqs. (2) and (12):

$$\mathcal{K}^{\alpha\beta}(p, k, P) = -\frac{Z_2^2}{4} \frac{\mathcal{G}(q^2)}{q^2} T_{\mu\nu}(q) \, \mathrm{tr}_{\mathrm{CD}} \left[P^\alpha(p, P) \gamma_\mu \lambda^a S(k_+) \mathcal{A}^\beta(k, P) S(k_-) \gamma_\nu \lambda^a \right] . \tag{7}$$

---

[1] see, e.g., Ref. [20] for the derivation of the change of basis coefficients $P^{\alpha\beta}(p, P)$.

In Eq. (6), $\lambda(P^2)$ is a scalar function and the eigenvalue equation has a solution for every value of P^2. Typically, iterative eigenvalue algorithms are employed as only under simplifying assumptions an inversion of the Bethe-Salpeter problem is possible [21–23]. To elucidate the iterative procedure, we simplify Eq. (6) (see also Ref. [24]), so that:

$$\lambda(P^2)\,|\Phi\rangle = \mathcal{K}(P^2)\,|\Phi\rangle \,. \tag{8}$$

The kernel, $\mathcal{K}(P^2)$, has a complete set of real eigenvectors ϕ_i with eigenvalues $\lambda_i(P^2)$ which are ordered as $\lambda_0(P^2) > \lambda_1(P^2) > \lambda_2(P^2) > .... > \lambda_i(P^2)$. Thus, any solution can be written as a linear superposition,

$$|\Phi\rangle = \sum_{i=1}^{\infty} a_i\,|\phi_i\rangle \,, \tag{9}$$

where a_i are real constants and the vector must be normalized. To begin the iterative process, one may "guess" as solution, such as in Eq. (9), for a given value of P^2 and n successive actions of the kernel lead to,

$$|\phi_n\rangle := \mathcal{K}^n(P^2)\,|\Phi\rangle = \sum_{i=1}^{\infty} \lambda_i^n a_i\,|\phi_i\rangle = \lambda_0^n \left[a_0\,|\phi_0\rangle + \sum_{i=1}^{\infty} \left(\frac{\lambda_i}{\lambda_0}\right)^n a_i\,|\phi_i\rangle \right] \,. \tag{10}$$

Since $\lambda_0 > \lambda_i$, the coefficients of $|\phi_i\rangle$ converge to zero for sufficiently large values of n and therefore the amplitude $|\phi_n\rangle$ converges to the ground state amplitude $|\phi_0\rangle$:

$$|\phi_n\rangle \overset{n\to\infty}{=} \lambda_0^n a_0\,|\phi_0\rangle \simeq \lambda_0\,\mathcal{K}^{n-1}(P^2)\,|\Phi\rangle \,. \tag{11}$$

This is the most basic method of computing the largest eigenvalue $\lambda_0(P^2)$ and its associated eigenvector to any required accuracy and is referred to as power or *von Mises* iteration. The trajectory of this eigenvalue function for a range of P^2 values yields the ground-state meson mass, that is one finds $\lambda_0(P^2) = 1$ when $P^2 = -m_0^2$.

2 Gram-Schmidt orthogonalization

A common procedure to extract the wave function of excited states from the spectrum of the interaction kernel is based on the Gram-Schmidt orthogonalization process. As mentioned in Section 1, the homogeneous Bethe-Salpeter equation is an eigenvalue problem, where the largest eigenvalue the interaction kernel produces corresponds to the ground state. However, the eigenvalue spectrum is not limited to the ground state and excited states with smaller eigenvalues can be determined with the same iterative methods discussed above. As sketched, e.g. in Ref. [24], one chooses a mass that is larger than the ground state mass, $P^2 = -m^2 < -m_0^2$, and applies the iterative procedure outlined in Section 1:

- find the largest eigenvalue, λ_0, and the associated eigenvector for $m^2 > m_0^2$ and $\lambda_0(m^2) > \lambda_0(m_0^2)$. This is the unphysical "ground state" at the mass scale $P^2 = -m^2$.

- make again a guess for the Bethe-Salpeter amplitude *now projecting out* the eigenvector that pertains to the largest eigenvalue $\lambda_0(m^2)$ in a first iteration.

- use the eigenvector obtained in the previous step as input for the Bethe-Salpeter amplitude and project out *again* the eigenvector associated with $\lambda_0(m^2)$ in a second iteration; the resulting eigenvector must be projected as before in a third iteration and so on.

- the iteration converges after the nth projection which yields an eigenvalue, $\lambda_1(m^2)$, with an eigenvector orthogonal to the one associated with the "ground state" eigenvalue $\lambda_0(m^2) > \lambda_1(m^2)$.
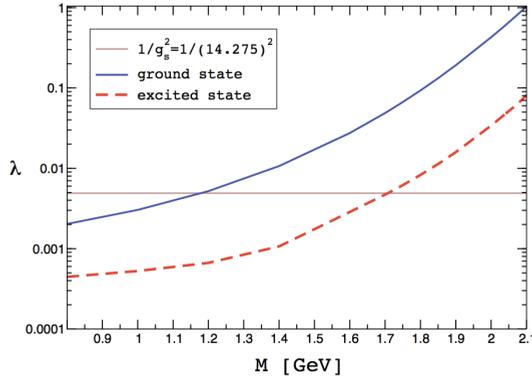
Figure 1. First two eigenvalue trajectories of the quark-diquark kernel used in Refs. [25, 26] as a function of $\sqrt{-P^2}$. Note that the eigenvector solutions are here differently normalized so that the eigenvalues are $\lambda_i = 1/g_s^2$ instead of $\lambda_i = 1$ for $P^2 = -m_i^2$; see Ref. [25] for details. The intersections of the solid horizontal line with the trajectories locates the mass-pole position of the nucleon and its first excited state identified with the *Roper*.

- by varying P^2 one obtains the mass evolution of the second largest eigenvalue $\lambda_1(P^2)$, which is exemplified in Figure 1. The solution for $\lambda_1(P^2) = 1$ yields the mass of the first excited state, $P^2 = -m_1^2$ where $m_1 > m_0$, at which the eigenvector is the state's Bethe-Salpeter amplitude.

The normalized projection within this Gram-Schmidt procedure is effected by,

$$|\tilde{\Phi}\rangle = |\Phi\rangle - \frac{\langle \phi_0 \,|\, \Phi \rangle}{\langle \phi_0 \,|\, \phi_0 \rangle} \, |\phi_0\rangle \,, \tag{12}$$

where $|\Phi\rangle$ is the initial guess for the Bethe-Salpeter amplitude in Eq. (3) and $|\phi_0\rangle$ is the vector of the ground-state Bethe-Salpeter amplitude. In projecting out this ground-state, one must define a norm in Euclidean space via an inner product, as is evident from Eq. (12). Within Quantum Field Theory in rainbow-ladder approximation, this product is defined as:

$$\langle \Psi \,|\, \Phi \rangle := \mathrm{tr}_{CD} \int_k^\Lambda \overline{\Psi}(k, -P)\, S(k + \eta_+ P)\, \Phi(k, p)\, S(k - \eta_- P) \,. \tag{13}$$

Orthogonality is thus defined by the condition, $\langle \Psi | \Phi \rangle = 0$, which expresses the vanishing of the overlap amplitude at P^2. Note that Eq. (13) is not valid for computations beyond the leading approximation, i.e. the rainbow-ladder truncation.

3 Krylov subspace and Arnoldi iteration

After momentum discretization and Chebyshev expansion of Eq. (6), the numerical kernel of the Bethe-Salpeter equation (or the Faddeev equation for the three-body problem) is a non-symmetric matrix of large dimensions and with some of its eigenvalues close to zero. In general, non-symmetric matrices have eigenvalues and eigenvectors which are very sensitive to small changes in the matrix elements due to the lack of symmetries on which traditional methods rely to ensure numerical stability [27]. This is particularly true for radial excitations, where angular dependence encoded in higher Chebyshev moments contributes in a nontrivial manner. Therefore, we make use of the numerical `ARPACK` library [28] which is designed to compute a few eigenvalues and corresponding eigenvectors

of a general $n \times n$ matrix by means of the implicitly restarted Arnoldi method (IRAM). The strength of the Arnoldi method [29] lies in the application of the stabilized orthogonalization algorithm in the Krylov space of a given matrix K to find its eigenvectors, as will be explained shortly. The most important feature of this algorithm is its ability to decouple the calculation of the eigenvectors corresponding to the eigenvalues with the largest absolute value from the eigenvectors whose eigenvalues have an absolute value close to zero. This is highly desirable as the calculation of the latter are plagued by numerical instabilities.

In algebra, the order-r Krylov subspace is generated by an operator whose representation is given by an $n \times n$ matrix $K = K_{ij}$, and a vector Φ of dimension n. It corresponds to the linear subspace spanned by actions of K on Φ:

$$\mathcal{S}_r := \left\{ \Phi, K\Phi, K^2\Phi, K^3\Phi, ..., K^{r-1}\Phi \right\} . \tag{14}$$

The power iteration of K yields the sequence in Eq. (14) and converges to the eigenvector associated with the largest eigenvalue λ_0. However, hereby one only makes very limited use of the stored information, as only the final vector, $K^{r-1}\Phi$, is kept. On the other hand, the basis for the Krylov subspace is derived from the Cayley-Hamilton theorem which implies that the inverse of a matrix can be expressed as a linear combination of its powers. Thus, Krylov subspaces play an important role in contemporary iterative methods to obtain one or few eigenvalues of large sparse matrices or to solve large systems of linear equations. Instead of heavy matrix operations, these methods rely on successive multiplications of vectors by the matrix, thus forming a Krylov subspace, and then employ the resulting vectors.

The vectors of the Krylov space are initially not ortogonal and usually become almost linearly dependent due to the properties of the matrix power iteration. Nonetheless, an orthogonal matrix can be constructed from the basis vectors by means of the Gram-Schmidt process described in Section 2. This method proves to be unstable but its shortcoming can be overcome with the Arnoldi iteration [29] which uses the *stabilized* Gram-Schmidt process and can be applied to general, possibly non-Hermitian matrices. The Arnoldi method generalizes the Gram-Schmidt process by computing the eigenvalues of the orthogonal projection of K onto the Krylov subspace, where the projection is represented by the upper Hessenberg matrix H_r [28]. For Hermitian (symmetric) matrices, the Arnoldi iteration is analogous to the Lanczos iteration.

4 A note on orthogonality

In the context of Bethe-Salpeter and Faddeev equations, orthogonality is defined by Eq. (13). In vectorial form, using the shorthand $x = k^2$ and $y = p^2$, Eq. (6) can be written as,

$$\lambda(y) \, \boldsymbol{F}_R(y) = \int dx \, \mathcal{K}(x, y) \cdot \boldsymbol{F}_R(x) , \tag{15}$$

which in a numerical treatment is evaluated as the sum,

$$\lambda(x_j) \, \boldsymbol{F}_R(x_j) = \sum_i w_i \, \mathcal{K}(x_j, x_i) \cdot \boldsymbol{F}_R(x_i) , \tag{16}$$

and similarly,

$$\lambda(x_j) \, \boldsymbol{F}_L(x_j) = \sum_i w_i \, \boldsymbol{F}_L(x_i) \cdot \mathcal{K}(x_j, x_i) , \tag{17}$$

where x_i are the nodes of a given quadrature with weights w_i. Since the integral in Eq. (13) is over a charge-conjugate Bethe-Salpeter amplitude, $\bar{\Psi}(k, -P) := C \, \Psi^T(-k, -P)C^T$, we introduce in Eqs. (16)

and (17) "left" and "right" eigenvectors, $\boldsymbol{F}_L$ and $\boldsymbol{F}_R$, respectively. Multiplying Eq. (16) from the left by $\sum_j w_j \boldsymbol{F}'_L(x_j)$ we obtain,

$$\lambda \sum_j w_j \boldsymbol{F}'_L(x_j) \cdot \boldsymbol{F}_R(x_j) = \sum_{i,j} w_i w_j \boldsymbol{F}'_L(x_j) \cdot \mathcal{K}(x_j, x_i) \cdot \boldsymbol{F}_R(x_i) = \lambda' \sum_i w_i \boldsymbol{F}'_L(x_i) \cdot \boldsymbol{F}_R(x_i) , \quad (18)$$

where $\boldsymbol{F}'_L(x_j)$ is the eigenvector associated with the eigenvalue λ'. For $\lambda \neq \lambda'$ this relation implies,

$$\int dx \, \boldsymbol{F}'_L(x) \cdot \boldsymbol{F}_R(x) = 0 , \quad (19)$$

The left eigenvector is given by the Bethe-Salpeter wave function, $S(k - \eta_- P) \overline{\Phi}_{\lambda'}(k, -P) S(k + \eta_+ P)$, and the right eigenvector is the Bethe-Salpeter amplitude [30]. We thus deduce from Eq. (19),

$$\mathrm{tr}_{\mathrm{CD}} \int_k S(k - \eta_- P) \overline{\Phi}_{\lambda'}(k, -P) S(k + \eta_+ P) \Phi_\lambda(k, P) = 0, \quad \text{for } \lambda' \neq \lambda , \quad (20)$$

and because the trace is cyclic this orthogonality condition is equivalent to that described in the paragraph below Eq. (13). Moreover, we verify that the Bethe-Salpeter equation spectrum of Eq. (16) is equal to that in Eq. (17). We stress that Eq. (19) is generally valid and no assumption was made about the kernel structure or about the eigenvectors.

5 Examples in hadron physics

The meson and nucleon resonance structure has been the object of a long history of studies and we here limit ourselves to the approaches based on the combined Dyson-Schwinger and Bethe-Salpeter (or Faddeev) equations, in particular their application to excited mesons and nucleons to compute their masses, weak decay constants and/or electromagnetic form factors making use of the techniques described in Sections 1–4.

Seminal studies on the ground state spectrum of light pseudoscalar mesons established that the $\pi(1300)$ can be described as the first radially excited state of the Goldstone boson and furthermore that the decay constant of excited states, P_n, vanishes identically in the chiral limit [31],

$$f_{P_n}^{\hat{m}=0}(\mu) \equiv 0 , \; n \geq 1 , \quad (21)$$

where $\hat{m}$ is the renormalization-group invariant current-quark mass. Electromagnetic properties of ground and excited state pseudoscalar mesons, making use of the the Gram-Schmidt process illustrated in Section 2, were studied in Ref. [32]. A first approach to computing the eigenvalues of unflavored light and heavy mesons and their corresponding Bethe-Salpeter amplitudes with the implicitly restarted Arnoldi factorization, as implemented in the `ARPACK` [28] library, is expounded in Refs. [30, 33] and has successively been applied to the light [35] and heavy [34, 35] quarkonia spectrum for pseudoscalar, vector and tensor states. A recent detailed analysis of the Maris-Tandy interaction [16] parameter space for ground and radially excited states is presented in Ref. [35], where the authors conclude that the preferred inverse effective range of the Maris-Tandy interaction in rainbow-ladder truncation, ω, is shorter for heavy quarkonia than for the light quarkonium spectrum: $\omega_{Q\bar{Q}} = 0.7$ GeV vs. $\omega_{q\bar{q}} = 0.5$ GeV.

The same library has then been employed to study radial excitations of flavor-singlet and flavored pseudoscalar mesons within the framework of the rainbow-ladder truncation [4, 36, 37]. A summary of the theoretical values for the pseudoscalar's ground- and excited-state masses and weak decay constants for flavor-singlet and nonsinglet $J^P = 0^-$ mesons is reproduced in Table 1 for two parameter

Table 1. Masses and decay constants for flavor singlet and nonsinglet $J^P = 0^-$ mesons; see Section 5.

	Model 1 [GeV]	Model 2 [GeV]	Reference
m_π	0.138	0.153	0.139 [38]
f_π	0.139	0.189	0.1304 [38]
$m_{\pi(1300)}$	0.990	1.414	1.30 ± 0.10 [38]
$f_{\pi(1300)}$	-1.1×10^{-3}	-8.3×10^{-4}	
m_K	0.493	0.541	0.493 [38]
f_K	0.164	0.214	0.156 [38]
$m_{K(1460)}$	1.158	1.580	1.460 [38]
$f_{K(1460)}$	-0.018	-0.017	
$m_{\bar{s}s}$	1.287	1.702	
$f_{\bar{s}s}$	-0.0214	-0.0216	
$m_{\eta_c(1S)}$	3.065	3.210	2.984 [38]
$f_{\eta_c(1S)}$	0.389	0.464	0.395 [39]
$m_{\eta_c(2S)}$	3.402	3.784	3.639 [38]
$f_{\eta_c(2S)}$	0.089	0.105	

sets of the interaction introduced by Qin et al. [17]. Namely, Model 1 and Model 2 correspond to the interaction parameters, $\omega = 0.4$ GeV, $\omega D = (0.8 \text{ GeV})^3$ and $\omega = 0.6$ GeV, $\omega D = (1.1 \text{ GeV})^3$; see Ref. [4] for details and Ref. [37] for a discussion of the effective interaction. Note that we explored a range of parameter combinations for $\omega D \neq$ const., yet could not find a unique set which produces theoretical observables that compare well with all data in Table 1. We therefore observe that we are unable to consistently and simultaneously describe both ground and excited state observables with the given interaction [2] in the rainbow-ladder truncation — whereas one parameter set successfully reproduces experimental ground state masses and decay constants but not the experimental data on excited states, the second parameter set only provides a reasonable description of the excited pseudoscalar mass spectrum.
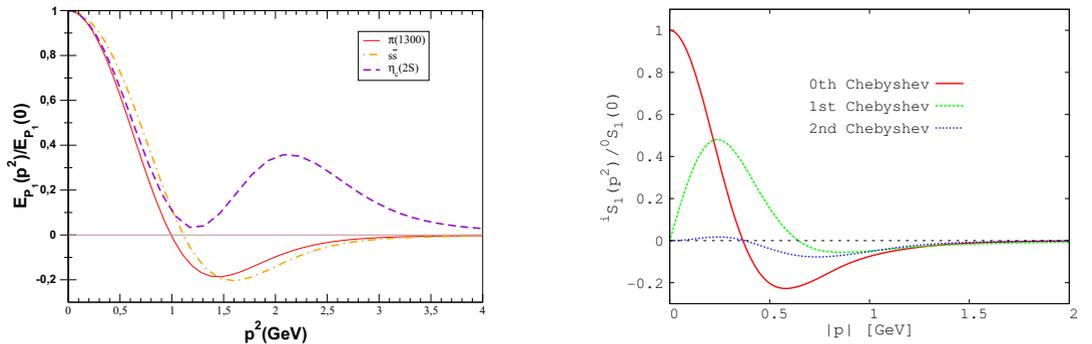

Figure 2. Left panel: Lowest Chebyshev moment, $^0E_{P_1}(p^2)$, associated with the leading Dirac structure $E_{P_1}(p^2)$ of the pseudoscalar's Bethe-Salpeter amplitude for the first radial excitations $P_1 = \pi(1300)$, $(\bar{s}s)_{n=1}$ and $\eta_c(2S)$. Right panel: First three normalized Chebyshev moments, $^iS_1(p^2)$, $i = 0, 1, 2$, of the leading S-wave component in the nucleon's first excited-state Faddeev amplitude.

As it becomes clear from the left graph of Fig. 2, for $p^2 \gtrsim 1$ GeV^2 the amplitude's lowest Chebyshev projection, $^0E_{P_1}(p^2)$ associated with the leading covariant $i\gamma_5$ of the pseudoscalar's Bethe-Salpeter amplitude, becomes negative definite in case of the first radial excitations, $\pi(1300)$ and $(\bar{s}s)_{n=1}$, whereas it remains positive for the ground states. It is remarkable that the behavior of the Bethe-Salpeter amplitudes parallels the pattern of wave functions in quantum mechanics, namely, the number of zeros can be associated with a principal quantum number n. As just mentioned, the ground state amplitude has no zeros and can thus be associated with $n = 0$. The amplitude of the next highest mass mesons possesses one zero and one assigns the quantum number $n = 1$ and so on. An analogous behavior is found for the nucleon's first excited state Faddeev amplitude for which we plot the first three Chebyshev moments of its leading S-wave component. Indeed, very recently a range of properties of the proton's radial excitation was predicted which strongly suggests that the nucleon's first radial excitation is the Roper resonance [26]. In particular, in Fig. 3 of Ref. [26] one can appreciate that the overlap amplitude between the nucleon and its first excited state described by the nucleon-Roper transition form factor $F_1^*(Q^2)$ vanishes at $Q^2 = 0$ and therefore satisfies orthogonality.

Acknowledgements

References

[1] A. Bashir, L. Chang, I. C. Cloët, B. El-Bennich, Y. X. Liu, C. D. Roberts and P. C. Tandy, Commun. Theor. Phys. **58**, 79 (2012).

[2] S. X. Qin, L. Chang, Y. X. Liu, C. D. Roberts and D. J. Wilson, Phys. Rev. C **85**, 035202 (2012).

[3] E. Rojas, J. P. B. C. de Melo, B. El-Bennich, O. Oliveira and T. Frederico, JHEP **1310**, 193 (2013).

[4] E. Rojas, B. El-Bennich and J. P. B. C. de Melo, Phys. Rev. D **90**, 074025 (2014).

[5] I. G. Aznauryan *et al.*, Int. J. Mod. Phys. E **22**, 1330015 (2013).

[6] B. El-Bennich, J. P. B. C. de Melo, B. Loiseau, J.-P. Dedonder and T. Frederico, Braz. J. Phys. **38**, 465 (2008).

[7] L. Chang, I. C. Cloët, B. El-Bennich, T. Klähn and C. D. Roberts, Chin. Phys. C **33**, 1189 (2009).

[8] E. O. da Silva, J. P. B. C. de Melo, B. El-Bennich and V. S. Filho, Phys. Rev. C **86**, 038202 (2012).

[9] B. El-Bennich, J. P. B. C. de Melo and T. Frederico, Few Body Syst. **54**, 1851 (2013).

[10] B. El-Bennich, M. A. Ivanov and C. D. Roberts, Nucl. Phys. Proc. Suppl. **199**, 184 (2010).

[11] B. El-Bennich, M. A. Ivanov and C. D. Roberts, Phys. Rev. C **83**, 025205 (2011).

[12] B. El-Bennich, G. Krein, L. Chang, C. D. Roberts and D. J. Wilson, Phys. Rev. D **85**, 031502 (2012).

[13] B. El-Bennich, C. D. Roberts and M. A. Ivanov, POS(QCD-TNT-II) 018, arXiv:1202.0454 [nucl-th] (2012).

[14] P. Maris, C. D. Roberts and P. C. Tandy, Phys. Lett. B **420**, 267 (1998).

[15] P. Maris and C. D. Roberts, Phys. Rev. C **56**, 3369 (1997).

[16] P. Maris and P. C. Tandy, Phys. Rev. C **60**, 055214 (1999).

[17] S. x. Qin, L. Chang, Y. x. Liu, C. D. Roberts and D. J. Wilson, Phys. Rev. C **84**, 042202 (2011).

[18] D. Binosi, L. Chang, J. Papavassiliou and C. D. Roberts, Phys. Lett. B **742**, 183 (2015).

[19] A. Bender, C. D. Roberts and L. Von Smekal, Phys. Lett. B **380**, 7 (1996).

[20] J. J. Cobos-Martínez, *Static and dynamic properties of the pion from continuum model ling of strong QCD*, PhD Thesis, Durham University (2010).

[21] W. Lucha and F. F. Schöberl, Phys. Rev. D **87**, no. 1, 016009 (2013).

[22] T. Frederico, G. Salmè and M. Viviani, Phys. Rev. D **89**, 016010 (2014).

[23] M. S. Bhagwat, A. Höll, A. Krassnigg, C. D. Roberts and S. V. Wright, Few Body Syst. **40**, 209 (2007).

[24] A. Krassnigg and C. D. Roberts, Fizika B **13**, 143 (2004).

[25] I. C. Cloët, G. Eichmann, B. El-Bennich, T. Klähn and C. D. Roberts, Few Body Syst. **46**, 1 (2009).

[26] J. Segovia, B. El-Bennich, E. Rojas, I. C. Cloët, C. D. Roberts, S. S. Xu and H. S. Zong, Phys. Rev. Lett. **115**, no. 17, 171801 (2015).

[27] W. H. Press, S. A. Teukolsky, W. T. Vetterling and B. P. Flannery, ISBN-9780521430647.

[28] R. B. Lehoucq, D. C. Sorensen, C. Yang, *ARPACK Users' Guide: Solution of Large-Scale Eigenvalue Problems with Implicitly Restarted Arnoldi Methods*, Siam (1998).

[29] W. E. Arnoldi, Quarterly of Applied Mathematics, vol. 9, pp. 17-29 (1951).

[30] M. Blank, arXiv:1106.4843 [hep-ph] (2011).

[31] A. Höll, A. Krassnigg and C. D. Roberts, Phys. Rev. C **70**, 042203 (2004).

[32] A. Höll, A. Krassnigg, P. Maris, C. D. Roberts and S. V. Wright, Phys. Rev. C **71**, 065204 (2005).

[33] M. Blank and A. Krassnigg, Comput. Phys. Commun. **182**, 1391 (2011).

[34] T. Hilger, C. Popovici, M. Gomez-Rocha and A. Krassnigg, Phys. Rev. D **91**, no. 3, 034013 (2015).

[35] T. Hilger, M. Gomez-Rocha and A. Krassnigg, arXiv:1508.07183 [hep-ph].

[36] B. El-Bennich, E. Rojas, M. A. Paracha and J. P. B. C. de Melo, AIP Conf. Proc. **1625**, 80 (2014).

[37] E. Rojas, B. El-Bennich, J. P. B. C. De Melo and M. A. Paracha, Few Body Syst. **56**, no. 6-9, 639 (2015).

[38] J. Beringer *et al.* [Particle Data Group Collaboration], Phys. Rev. D **86**, 010001 (2012).

[39] C. T. H. Davies, C. McNeile, E. Follana, G. P. Lepage, H. Na and J. Shigemitsu, Phys. Rev. D **82**, 114504 (2010).